extrahepatic vessel occluded is the right inferior phrenic artery (RIPA) (4,5).

This report received Institutional Review Board approval. A 72-year-old woman presented with an intrahepatic cholangiocarcinoma that affected segments I and IV (**Fig a**). As no contraindications were found, it was decided to perform ^{90}Y RE with resin microspheres (Sirtex Medical Europe GmbH, Bonn, Germany). Angiographic work-up demonstrated that a small part of the tumor was vascularized by the RIPA (**Fig b**). Because of this, the RIPA was proximally occluded with microcoils with the aim to redistribute its vascular territory to treat the whole tumor volume from the intrahepatic branches. Combined technetium 99m–labeled macroaggregated albumin single photon emission computed tomography/computed tomography (CT) was performed and did not show any extrahepatic uptake or high lung shunt fraction. Therefore, 1 week later, the treatment was administered using 2 different injection points, 1 from the segment VII artery (1 GBq) and 1 from the segment IV artery (1 GBq). Positron emission tomography (PET)/CT performed 20 hours after the treatment demonstrated good ^{90}Y uptake in the tumor; however, high uptake was also shown in the posteroinferior segment of the right lung (**Fig c**).

The patient was asymptomatic and was discharged 24 hours after ^{90}Y RE. She received 2 cycles of gemcitabine and cisplatin 1 month later. CT scan performed 3 months after ^{90}Y RE showed that the tumor was partially decreased in size in the right lobe, but clear progression of tumor was detected in the left lobe. A fibrotic scar was detected in the area of ^{90}Y PET/CT uptake in the right lung (**Fig d**). The patient did not show any sign of pulmonary complications (no dyspnea). She died of liver tumor progression 4 months after ^{90}Y RE.

The images suggest that, owing to the intratumoral arterial connections, the most distal branches of the proximally occluded RIPA were retrogradely vascularized. Hence, it may be inferred that the distal (phrenic) arteries may have been loaded with ^{90}Y microspheres. Furthermore, the presence of the segmental diaphragmatic defect (even without any transdiaphragmatic herniation) allowed direct passage of microspheres toward the neighboring parietal pleura resulting in direct radiation of the surrounding lung parenchyma. As Kinoshita et al (6) pointed out, these diaphragmatic defects "are a common finding on multidetector-row computed tomography, occurring in up to 20% of persons by age 70 years."

Three conclusions can be drawn from this case. First, a focal uptake in a small area of nonproliferative tissues (lung), with low functional impact, may not significantly affect the patient. Second, the diaphragmatic defect, being common and asymptomatic, must be taken into consideration in cases in which the tumor is fed by the RIPA. Third, negative morphologic consequences (extended fibrotic scar) may arise from massive radiation of the lung parenchyma if a significant number of ^{90}Y microspheres reach the lung owing to a high lung shunt fraction (not present in this case).

REFERENCES

1. Wright CL, Werner JD, Tran JM, et al. Radiation pneumonitis following yttrium 90 radioembolization: case report and literature review. J Vasc Interv Radiol 2012; 23:669–674.
2. Leung TW, Lau WY, Ho SK, et al. Radiation pneumonitis after selective internal radiation treatment with intraarterial 90 yttrium-microspheres for inoperable hepatic tumors. Int J Radiat Oncol Biol Phys 1995; 33: 919–924.
3. Sangro B, Martínez-Urbistondo D, Bester L, et al. Prevention and treatment of complications of selective internal radiation therapy: expert guidance and systematic review. Hepatology 2017; 66:969–982.
4. Tajima T, Honda H, Kuroiwa T, et al. Pulmonary complications after hepatic artery chemoembolization or infusion via the inferior phrenic artery for primary liver cancer. J Vasc Interv Radiol 2002; 13:893–900.
5. Miyayama S, Matsui O, Taki K, et al. Extrahepatic blood supply to hepatocellular carcinoma: angiographic demonstration and transcatheter arterial chemoembolization. Cardiovasc Intervent Radiol 2006; 29: 39–48.
6. Kinoshita F, Ishiyama M, Honda S, et al. Late-presenting posterior transdiaphragmatic (Bochdalek) hernia in adults: prevalence and MDCT characteristics. J Thorac Imaging 2009; 24:17–22.

Rapid Development of New Aneurysms in the Adjacent Pancreatic Arcade Arteries after Urgent Embolization of Pancreaticoduodenal Artery Aneurysms in Cases with Celiac Stenosis

From: Tetsuya Hasegawa, MD, PhD
Kazumasa Seiji, MD, PhD
Hideki Ota, MD, PhD
Tomonori Matsuura, MD, PhD
Nozomi Satani, MD, PhD
Tomomi Sato, MD, PhD
Kei Takase, MD, PhD
Department of Diagnostic Radiology (T.H., N.S., K.T.)
Tohoku University Graduate School of Medicine
1-1 Seiryo-machi, Aoba-ku, Sendai, Miyagi, 980-8574
Japan; and
Department of Diagnostic Radiology (K.S., H.O., T.M., T.S.)
Tohoku University Hospital
Sendai, Miyagi, Japan

Editor:

The frequency of pancreaticoduodenal arcade aneurysms is reportedly approximately 2% of all visceral artery aneurysms (1). Celiac artery stenosis or occlusion due to the median arcuate ligament is the main cause of true aneurysm

None of the authors have identified a conflict of interest.

Figures E1 and E2 are available online at *www.jvir.org*.

https://doi.org/10.1016/j.jvir.2018.04.003

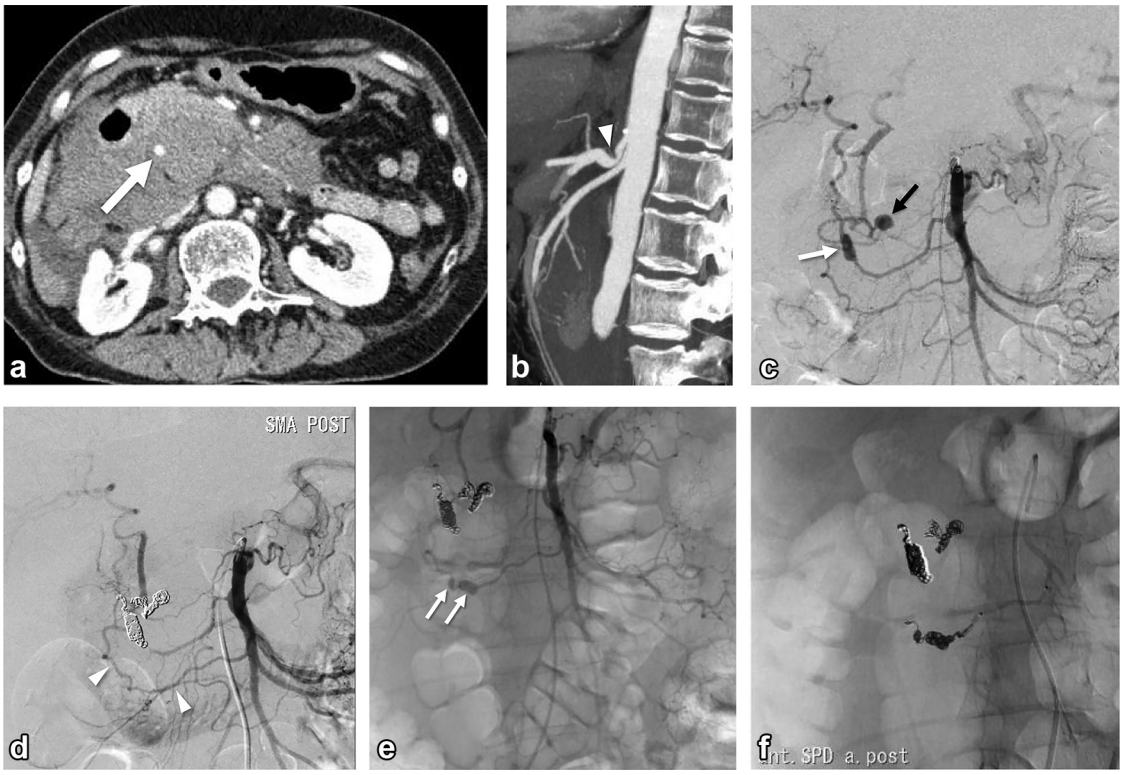

Figure. (**a**) Axial CECT section through the level of the pancreas in a 59-year-old woman with sudden onset of stomach pain and hypotension. A 5.4-mm-diameter hyper-attenuating arterial contrast (arrow) is seen within the peripancreatic hematoma, representing 1 of the 2 aneurysms of the pancreaticoduodenal arcades, as demonstrated on the superior mesenteric digital subtraction angiogram. (**b**) Sagittal MIP image obtained in full expiration shows a characteristic concave impression on the cranial surface of the celiac artery just beyond its origin (arrowhead). (**c**) Pancreaticoduodenal aneurysms arising from the posterior pancreatic arcade (white arrow) and the proximal gastroepiploic artery (black arrow). The transverse pancreatic artery arises from the proximal SMA and fills the pancreatica magna and the splenic artery. (**d**) Superior mesenteric angiogram after coil embolization of the aneurysms of the gastroepiploic artery and posterior pancreatic arcade demonstrates occlusion of the aneurysms. There is collateral supply to the liver through the anterior pancreaticoduodenal arcade (arrowheads). (**e**) Digital superior mesenteric angiogram 27 hours after the initial embolization shows 2 new aneurysms (white arrows) arising from the previously patent AIPD artery. (**f**) Digital angiogram with the injection of contrast medium into the inferior pancreatic arcade after the embolization shows occlusion of the aneurysm and feeding artery.

formation in the pancreaticoduodenal arcades (2). This report presents the cases of 2 such patients with rapid aneurysm formations in the adjacent pancreatic arcades after pancreatic arcades aneurysm embolization.

The first patient was a 59-year-old otherwise healthy woman who had sudden upper-right abdominal pain. Upon arrival, her blood pressure and pulse were 90/58 mmHg and 90 beats/minute, respectively. Laboratory tests showed white blood cell (WBC) count of 11,300/μL (reference value [RV]: 3,300–8,600/μL); C-reactive protein (CRP) level of 8.7 mg/dL (RV: <0.14 mg/L); hemoglobin of 7.6 g/dL (RV: 11.6–14.8 g/dL); and serum amylase of 106 U/L (RV: 44–132 U/L). Contrast-enhanced computed tomography (CECT) showed a large retroperitoneal (peripancreatic) hematoma and an aneurysm (**Fig a**). Sagittal maximum-intensity projection (MIP) imaging revealed severe stenosis of the celiac axis due to compression by the median arcuate ligament and post-stenotic dilatation (**Fig b**). Superior mesenteric digital subtraction angiography showed superior mesenteric to hepatic artery collaterals through dilated pancreaticoduodenal arcades. Small aneurysms were seen on the posterior superior pancreaticoduodenal artery (13.9 mm) and right gastroepiploic artery (9.8 mm) (**Fig c**). No abnormality was observed in the anterior arcade. Celiac arteriography showed a flow defect in the common hepatic artery and did not fill the pancreatic arcades due to flow reversal in the gastroduodenal artery. The aneurysms were occluded with 8 3–8-mm Tornado coils (Cook Medical, Bloomington, Indiana) and 4 4–5-mm VortX Diamond coils (Boston Scientific, Natick, Massachusetts). A post-embolization superior mesenteric angiogram revealed that both aneurysms did not fill with contrast medium, and that the hepatic artery filled through the anterior arcades from the superior mesenteric artery (SMA) and the splenic artery from the pancreatic branches of the SMA (**Fig d**). However, 27 hours after embolization, the patient complained of epigastric pain and a drop in blood pressure to 88/50 mmHg. Repeat CECT showed development of a new aneurysm measuring 8.9 mm in diameter in the retroperitoneal hematoma (**Fig E1** [available online at *www.jvir.org*]). Repeat SMA angiography showed development of 2 new aneurysms measuring 10.3 mm and 6.0 mm in the anterior inferior pancreaticoduodenal